Numerical modeling of rudder sheet cavitation including propeller/rudder interaction and the effects of a tunnel

Hanseong Lee
Ocean Engineering Group
The University of Texas at Austin, USA
hslee@mail.utexas.edu

Spyros A. Kinnas
Ocean Engineering Group
The University of Texas at Austin, USA
kinnas@mail.utexas.edu

Hua Gu
Ocean Engineering Group
The University of Texas at Austin, USA
guhua@mail.utexas.edu

Shreenaath Natarajan
Ocean Engineering Group
The University of Texas at Austin, USA
shreenaath@mail.utexas.edu

ABSTRACT

This paper presents the coupling of a vortex lattice method (MPUF-3A), a finite volume method (GBFLOW-3D), and a boundary element method (PROPCAV) to allow for the prediction of rudder sheet cavitation, including the effect of propeller, as well as the effects of tunnel walls.

The unsteady cavity prediction on the propeller blades is performed using MPUF-3A to satisfy both a constant pressure condition on the cavity surface and the flow tangency condition on the cavity and blade surfaces. The effects of the tunnel and a vortical inflow are modeled via GBFLOW-3D by solving the 3-D Euler equations with slip boundary conditions on the walls and by representing the effect of the propeller blades via body forces.

The cavity prediction on the rudder is accomplished via PROPCAV (which can handle back and face leading edge or mid-chord cavitation) in the presence of the 3-D flow field produced by the propeller. This flow-field is determined via GBFLOW-3D, in which the propeller is represented via a non-axisymmetric distribution of body forces. The effects of the tunnel walls are also considered in this case by applying a boundary element method on the walls, in the presence of the rudder.

A multi-block Euler scheme is also developed in order to determine the effect of the rudder on the propeller inflow.

The present method is first validated by performing convergence studies on a cavitating rudder with varying number of panels. Then, the predicted cavity shapes on a (horn-type) rudder downstream of a propeller are compared to those observed in a experiment performed in a cavitation tunnel.

INTRODUCTION

Rudders operate in the stern of a ship behind the propeller slipstream, and are subjected to an accelerated and swirled inflow induced by the hull and the propeller. The swirled flow induced by the propeller increases the angle of attack to some parts of the rudder, and as a result the loading of the rudder increases, and sheet cavitation often appears over the rudder surface. Therefore, the interaction between the propeller and the rudder is very important for the analysis of both devices.

There have been a lot of numerical methods, based on potential theory, which predict the cavitating performance of a propeller or a hydrofoil (rudder). Two methods, i.e., a vortex lattice method (VLM) and a boundary element method (BEM), have been successfully applied to the sheet cavity prediction.

Previous work

A vortex lattice method was first applied to the analysis of unsteady fully wetted performance of a marine propeller subject to non-uniform inflows by [Kerwin and Lee 1978]. Later, their method was extended to analyze 3-D unsteady sheet cavitation using the linearized cavity theory by [Lee 1979, 1981; Breslin et al. 1982]. However, the linear theory predicts longer cavity extent as the blade thickness increases, which is contrary to the non-linear theory [Uhlman 1987] as well as the short cavity theory [Tulin and Hsu 1980]. [Kerwin et al. 1986] modified the method of [Lee 1979, 1981; Breslin et al. 1982] to take into account the non-linear blade thickness effect by implementing the leading edge correction [Kinnas 1985, 1991]. [Kinnas and Fine 1989] extended the method to predict unsteady partial cavity with prescribed mid-chord and/or face

cavity detachment, and [Kudo and Kinnas 1995] extended the method to treat super-cavitating propellers subject to steady flow. Recently, the method was named MPUF-3A by including the ability to search for mid-chord cavitation [Kinnas et al. 1998a, 1999]. The latest version of MPUF-3A [Lee et al. 2003] includes the effect of hub, non-linear thickness-loading coupling, and wake alignment in uniform and inclined inflow.

The boundary element method has been widely used for the prediction of sheet cavitation due to the defect of the linear theory in the vortex lattice method. A non-linear potential based boundary element method was first applied for the analysis of a cavitating propeller subject to non-axisymmetric inflows by [Fine 1992; Kinnas and Fine 1992; Fine and Kinnas 1993b], and for the analysis of the cavitating hydrofoils by [Kinnas and Fine 1993; Fine and Kinnas 1993a]. Their method, named PROP-CAV, discretizes the exact blade surface and places constant strength of dipole and source distributions on the discretized panels. Thus, this method predicts more accurately the pressures and cavity patterns at the propeller leading edge, trailing edge and tip where the linear cavity theory breakdowns in the vortex lattice method. PROP-CAV was extended to predict the face and/or back cavitation with searched cavity detachment by [Kinnas et al. 1997; Mueller and Kinnas 1997; Mueller 1998; Mueller and Kinnas 1999], and to treat the mixed partial and super-cavity on both face and/or back sides of the blade simultaneously by [Young and Kinnas 1999, 2001]. PROPCAV was further extended to treat super-cavitating propellers with finite thickness trailing edge as well as surface piercing propellers by [Young 2002; Young and Kinnas 2002, 2003]. The treatment of a developed tip vortex cavity and a procedure for the fully unsteady wake alignment were also incorporated in PROPCAV by [Lee and Kinnas 2001; Lee 2002; Lee and Kinnas 2003]. [Kinnas et al. 1998b, 2000] applied a boundary element method to analyze the cavitating flow over 3-D hydrofoil subject to a uniform inflow inside a circular tunnel, and the interaction between hydrofoil and tunnel wall was determined in an iterative manner.

The accurate prediction of the effective wake is very crucial in determining the propeller loading and the flow field induced by the propeller over the rudder downstream. [Choi and Kinnas 1998; Kinnas et al. 2000; Choi and Kinnas 2001] applied a finite volume method to predict the 3-D effective wake of single propeller in unbounded or inside of a circular section tunnel. A three-dimensional unsteady Euler solver based on a finite volume approach and the pressure correction method, was developed to predict the unsteady effective wake for propellers subject to non-axisymmetric inflows by [Choi and Kinnas 2000a,b; Choi 2000; Choi and Kinnas 2003]. Recently, [Kinnas et al. 2003; Natarajan 2003] extended the 3-D Euler solver to include the effect of a non-axisymmetric strut and pod, and to evaluate the flow field over the rudder induced by the propeller.

The hydrodynamic interaction between propeller and rudder is of great importance because of its effect on the performance of both. [Tamashima et al. 1993] used a simplified propeller theory, which treats the propeller as an actuator disc, to calculate the performance of the propellers, and a panel method to calculate the forces acting on the rudder. In [Han et al. 1999], they developed a numerical technique using boundary element method to analyze the propeller-rudder interaction, and the calculated results were compared with the measured from experiments. [Shen et al. 1997] performed a series of experiments to study the effect of ship hull and propeller on the rudder cavitation, and compared the measured pressure distribution over the rudder with those predicted by a panel method. [Han et al. 2001] used a surface panel method to solve the flow around a horn-type rudder and a vortex-lattice method to solve the flow around the propeller, respectively. The three-dimensional flow around the rudder and the propeller was computed simultaneously, considering the interactions between the two. In [Achkinadze et al. 2003], a velocity based boundary element method has been applied to predict the rudder forces subject to the non-axisymmetric inflow to the rudder induced by propeller.

Present work

In the present work, a vortex lattice method (MPUF-3A), a three-dimensional Euler solver (GBFLOW-3D), and a boundary element method (PROPCAV) are coupled to predict sheet cavitation on rudder with the effects of propeller and tunnel. The inflow to a rudder is evaluated using GBFLOW-3D which is coupled with MPUF-3A to compute the body forces which represent the propeller in 3-D Euler solver. In GBFLOW-3D, the hull, tunnel and hub are treated as solid boundaries, however, the rudder is not represented by either body forces or a solid boundary. The cavity prediction on the rudder is performed using PROP-CAV based on the inflow evaluated from GBFLOW-3D. In addition, the tunnel walls are modeled via a boundary element method and coupled with PROPCAV to include the effects of tunnel walls. A multi-block scheme is also developed to evaluated the effect of rudder on the propeller by using an Euler solver, in which the rudder is modeled as a part of solid boundary.

FORMULATION

Cavitating rudder inside a tunnel

Consider a 3-D cavitating/non-cavitating rudder subject to a general inflow $\vec{q}_{in}$, inside of a tunnel, as shown in
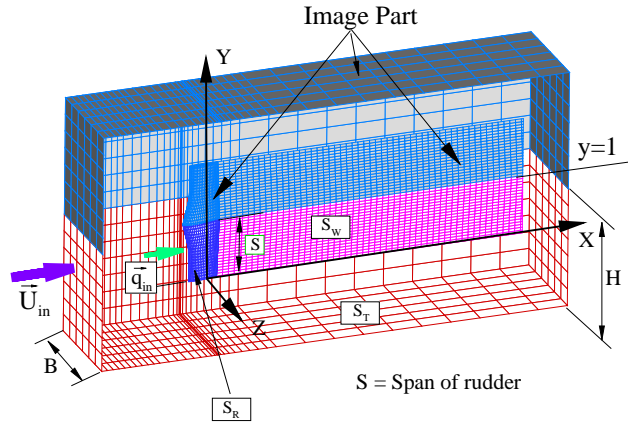
Figure 1: Computational domain showing tunnel, rudder and wake geometries. The images of the tunnel, rudder and wake are shown at the top half of the domain ($y > 1$).

Fig. 1. The inflow onto rudder, $\vec{q}_{in}$, is determined by considering the interaction between propeller and rudder using a three-dimensional Euler solver (GBFLOW-3D) and a vortex lattice method (MPUF-3A).

Assume that the flow around the rudder is inviscid, irrotational and incompressible, so that the fluid domain can be represented via the perturbation potential, $\phi(x,y,z)$, expressed as follows:

$$\vec{q}(x,y,z) = \vec{q}_{in}(x,y,z) + \nabla\phi(x,y,z) \qquad (1)$$

where $\vec{q}(x,y,z)$ is the total velocity vector, and the perturbation potential, $\phi(x,y,z)$, satisfies the Laplace's equation in the fluid domain.

$$\nabla^2\phi(x,y,z) = 0 \qquad (2)$$

The perturbation potential, $\phi(x,y,z)$, at every point $p(x,y,z)$ on the rudder, wake and tunnel surface, $S_R \cup S_W \cup S_T$, must satisfy Green's third identity:

$$
\begin{aligned}
2\pi\phi &= \int\int_{S_R}\left[\phi_q\frac{\partial G(p;q)}{\partial n_q} - G(p;q)\frac{\partial\phi_q}{\partial n_q}\right]ds \\
&+ \int\int_{S_W}\Delta\phi_q\frac{\partial G(p;q)}{\partial n_q}ds \\
&+ \int\int_{S_T}\left[\phi_q\frac{\partial G(p;q)}{\partial n_q} - G(p;q)\frac{\partial\phi_q}{\partial n_q}\right]ds
\end{aligned}
\qquad (3)
$$

where the subscript q corresponds to the variable point in the integration, and $G(p;q) = 1/R(p;q)$ is the Green's function with $R(p;q)$ being the distance between points p and q. $\vec{n}$ is the unit vector normal to the integration surface

defined as a positive direction when pointing into fluid domain.

Eventhough the integral equation, given in Eqn. 3, can be solved directly by considering the rudder and the tunnel as a part of the same boundary, an iterative method is adopted in the present method [Kinnas et al. 1998b]. The method is composed of two parts, the rudder and the tunnel parts, which are solved successively while the interaction is taken into account iteratively through the induced potential of each one on the other.

Consider the induced potential on the rudder due to the tunnel wall (ϕ^T), and the induced potential on the tunnel wall due to the rudder (ϕ^R).

$$4\pi\phi^T = \int\int_{S_T}\left[\phi_q\frac{\partial G(p;q)}{\partial n_q} - G(p;q)\frac{\partial\phi_q}{\partial n_q}\right]ds \qquad (4)$$

$$
\begin{aligned}
4\pi\phi^R &= \int\int_{S_R}\left[\phi_q\frac{\partial G(p;q)}{\partial n_q} - G(p;q)\frac{\partial\phi_q}{\partial n_q}\right]ds \\
&+ \int\int_{S_W}\Delta\phi_q\frac{\partial G(p;q)}{\partial n_q}ds
\end{aligned}
\qquad (5)
$$

From Eqn. 3 and 4, the integral equation for the external flow around the rudder is given as follows;

$$
\begin{aligned}
2\pi\phi &= \int\int_{S_R}\left[\phi_q\frac{\partial G(p;q)}{\partial n_q} - G(p;q)\frac{\partial\phi_q}{\partial n_q}\right]ds \\
&+ \int\int_{S_W}\Delta\phi_q\frac{\partial G(p;q)}{\partial n_q}ds + 4\pi\phi^T
\end{aligned}
\qquad (6)
$$

The integral equation for the internal flow inside the tunnel is obtained by substituting Eqn. 5 into Eqn. 3.

$$
\begin{aligned}
2\pi\phi &= \int\int_{S_T}\left[\phi_q\frac{\partial G(p;q)}{\partial n_q} - G(p;q)\frac{\partial\phi_q}{\partial n_q}\right]ds \\
&+ 4\pi\phi^R
\end{aligned}
\qquad (7)
$$

Equations 6 and 7 can be solved iteratively by applying the boundary conditions via a boundary element method, and the interaction terms, ϕ^T and ϕ^R, are updated during the iterative process.

Boundary conditions on tunnel walls

Assume that the inflow velocity, $\vec{U}_{in}$, to the tunnel is uniform and coming from far upstream [Kinnas et al. 1998b].

- Flow tangency condition on solid tunnel walls : the flow normal to the tunnel wall is equal to zero.

$$\frac{\partial\phi}{\partial n} = 0 \qquad (8)$$

- Inflow and outflow boundary conditions: the total velocity normal to the inlet/outlet boundaries is equal to uniform inflow, $\vec{U}_{in}$.

$$\vec{U}_{in} \cdot \vec{n} + \nabla\phi \cdot \vec{n} = \vec{U}_{in} \cdot \vec{n}$$
$$\text{or} \quad \frac{\partial\phi}{\partial n} = 0 \quad\quad (9)$$

Boundary conditions on cavitating rudder

Figure 2 shows boundary conditions on cavitating rudder, and the definition of local coordinates. The applied boundary conditions are as follows:

- Kinematic boundary condition on wetted surface: the flow is tangent to the rudder surfaces.

$$\frac{\partial\phi}{\partial n} = \vec{q}_{in} \cdot \vec{n} \quad\quad (10)$$

- Kutta condition: the velocity at the rudder trailing edge has to be finite.

$$|\nabla\phi| < \infty \quad\quad \text{at T.E.} \quad\quad (11)$$

- Cavity closure condition: the cavity closes at the cavity end. This condition requires iterative solution method to find the cavity planform [Kinnas and Fine 1993].

$$\delta(l, \sigma) = 0 \quad\quad (12)$$

where δ is the cavity height at the cavity trailing edge and is a function of cavity length, l, and cavitation number, σ.

- Kinematic boundary condition on cavity surface: the total velocity normal to the cavity surface requires to be zero. The kinematic boundary condition leads to the following partial differential equation for the cavity height calculation [Kinnas and Fine 1993].

$$\frac{\partial h}{\partial s}\left[V_s - \cos\psi V_v\right] + \frac{\partial h}{\partial v}\left[V_v - \cos\psi V_s\right] = V_n\sin^2\psi$$
$$(13)$$

where h is the cavity height normal to the rudder surface. s, v and n denote the non-orthogonal curvilinear coordinates defined on rudder surface, and V_s, V_v and V_n are the total velocities of s, v and n directions, respectively.

- Dynamic boundary condition on cavity surface: the dynamic boundary condition on the cavitating rudder and wake surfaces requires the pressure everywhere on the cavity to be constant and equal to the vapor pressure, P_v. Since Bernoulli's constant increases
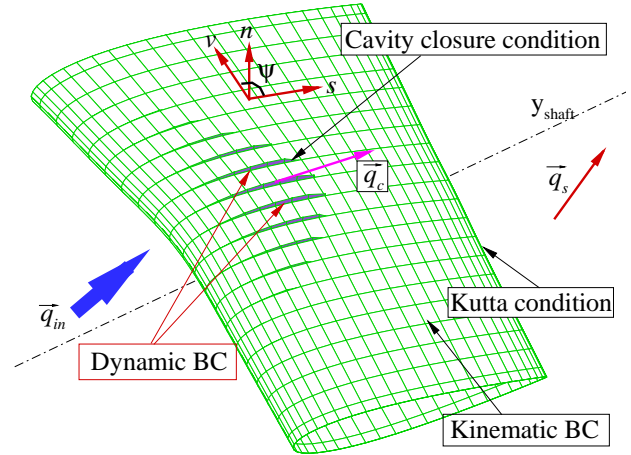

Figure 2: Boundary conditions on cavitating rudder subject to the propeller induced inflow, and the definition of local coordinates.

across the propeller plane, Bernoulli's equation cannot directly apply between points on the rudder and the points upstream of the propeller. In the present work, Bernoulli's equation is applied between a point on the cavity surface with a vertical coordinate, y, and a point with a vertical coordinate, y_s, far downstream along the same streamline where the velocity magnitude is q_s and the pressure p_s [Kinnas et al. 2003; Natarajan 2003]. The velocity q_s and the pressure p_s far downstream are determined from GBFLOW-3D.

$$p_v + \frac{\rho}{2}q_c^2 + \rho g y = p_s + \frac{\rho}{2}q_s^2 + \rho g y_s \quad\quad (14)$$

Since the pressure variation far downstream, as predicted by GBFLOW-3D (in which the pressures do not include the hydrostatic pressure) is small[†] as described in [Kinnas et al. 2003; Natarajan 2003], we can assume that the pressure far downstream is practically only due to hydrostatic effects.

$$p_v + \frac{\rho}{2}q_c^2 + \rho g y = p_{shaft} + \frac{\rho}{2}q_s^2 + \rho g y_{shaft} \quad (15)$$

where p_{shaft} is the absolute pressure at the propeller shaft axis and y_{shaft} is the vertical coordinate of the shaft axis.

By combining Eqn. 14 and 15 and non-dimensionalizing with $\rho V_{ship}^2/2$, the cavity velocity on the rudder is defined as following:

[†]The range of the pressures predicted by GBFLOW-3D can also be seen in Fig.19.

$$\frac{q_c}{V_{ship}} = \sqrt{\left(\frac{q_s}{V_{ship}}\right)^2 + \sigma(y)} \qquad (16)$$

where V_{ship} is the ship speed. $\sigma(y)$ is the *local cavitation number* at a vertical coordinate y and is given as:

$$\sigma(y) = \sigma_R - 2g\frac{y - y_{shaft}}{V_{ship}^2} \qquad (17)$$

and the rudder cavitation number σ_R is,

$$\sigma_R = \frac{p_{shaft} - p_v}{\frac{\rho}{2}V_{ship}^2} \qquad (18)$$

From Bernoulli's equation and the definition of total cavity velocity on the non-orthogonal local coordinates, the expression for the unknown chordwise perturbation velocity, $\frac{\partial\phi}{\partial s}$, can be derived with assumption that $\vec{q}_s$ is equal to $\vec{q}_{in}$:

$$\frac{\partial\phi}{\partial s} = -\vec{q}_{in}\cdot\vec{s} + V_v\cos\psi + \sin\psi\sqrt{q_c^2 - V_v^2} \quad (19)$$

where ψ is the angle between s and v directions.

Equation 19 is integrated to form a Dirichlet type boundary condition for perturbation potential ϕ over the cavity surface [Kinnas and Fine 1993].

- Cavity detachment condition: the cavity detachment location is determined iteratively until the following *smooth detachment condition* is satisfied [Young 2002].

  1. The cavity has non-negative thickness at its leading edge.
  2. The pressure on the wetted portion of the rudder upstream of the cavity should be greater than the vapor pressure.

Three-dimensional steady Euler solver

A three-dimensional steady Euler solver, named GBFLOW-3D, is used to solve the flow around the propeller and tunnel in the absence of rudder. GBFLOW-3D uses a finite volume method and the artificial compressibility method [Chorin 1967]. The details on this method are described in [Choi 2000; Choi and Kinnas 2001].

The dimensionless continuity and the momentum equations can be expressed as following:

$$\frac{\partial \mathbf{U}}{\partial t^*} + \frac{\partial \mathbf{F}}{\partial x} + \frac{\partial \mathbf{G}}{\partial y} + \frac{\partial \mathbf{H}}{\partial z} = \mathbf{Q} \qquad (20)$$

where $\mathbf{U}$, $\mathbf{F}$, $\mathbf{G}$, $\mathbf{H}$, and $\mathbf{Q}$ are defined as follows.

$$
\mathbf{U} = \begin{bmatrix} p \\ u \\ v \\ w \end{bmatrix}, \quad
\mathbf{F} = \begin{bmatrix} u/\beta \\ u^2 + p \\ uv \\ uw \end{bmatrix},
$$

$$
\mathbf{G} = \begin{bmatrix} v/\beta \\ uv \\ v^2 + p \\ vw \end{bmatrix}, \quad
\mathbf{H} = \begin{bmatrix} w/\beta \\ uw \\ vw \\ w^2 + p \end{bmatrix},
$$

$$
\mathbf{Q} = \begin{bmatrix} 0 \\ f_x \\ f_y \\ f_z \end{bmatrix} \qquad (21)
$$

where β is the artificial compressibility factor. A vertex based scheme [Choi and Kinnas 2001], Ni's lax-Wendroff method [Ni 1982] for the time discretization, and a fourth order artificial viscosity were adapted to solve the governing equation (Eqn. 20).

The body force distribution on the finite volume cells which correspond to the location of blade can be obtained by the integration of the pressure difference across the blade surface, Δp, over the area of the lifting surface. The dimensionless three-dimensional body force can be calculated by the following formula [Choi and Kinnas 2001].

$$\vec{f}_{3D} = \left(\frac{4}{\mathcal{V}_c J_s^2}\right)\vec{F}_P \qquad (22)$$

where $\vec{F}_P$ is the dimensionless pressure force obtained from the propeller potential flow solver (MPUF-3A). $\mathcal{V}_c$ is the cell volume, and J_s is the advance ratio based on ship speed. In [Choi and Kinnas 2001] the body force was varied in the circumferential direction according to the propeller loading at the same blade angle. This body force can be considered as the time average of the body force at a point in space in the case of non-axisymmetric nominal inflow.

Boundary conditions

The boundaries of computational domain and the applied boundary conditions in Euler solver are shown in Fig. 3. Eventhough the rudder is shown in Fig. 3, the rudder is not modeled in Euler solver. The boundary conditions applied in this problem are as follows:

- Upstream boundary: the velocities are equal to the given values, and the derivative of the pressure with respect to the axial direction is set to zero.

$$(u, v, w) = (u, v, w)_{given} \qquad (23)$$

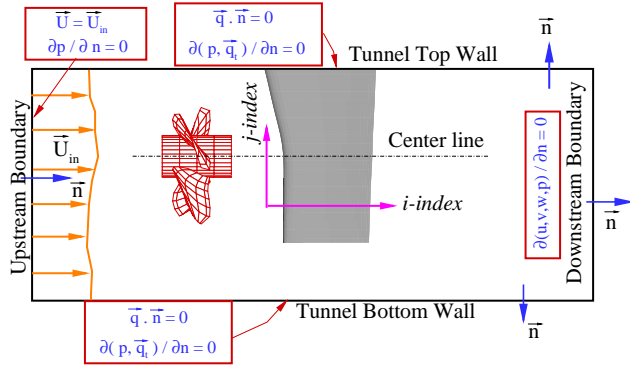$$\frac{\partial p}{\partial n} = \frac{\partial p}{\partial x} = 0 \qquad (24)$$

Figure 3: Boundary conditions for the Euler solver, and propeller and rudder arrangement in computational domain: $\vec{q} = (u, v, w)$ is the total velocity. $\vec{q}_t$, and $\vec{q}_n$ are the tangential and the normal components of the total velocity, i.e. $\vec{q} = \vec{q}_n + \vec{q}_t$.

- Downstream boundary: the first derivatives of the velocities and the pressure with respect to axial direction are set to zero.

$$\frac{\partial(u, v, w, p)}{\partial n} = \frac{\partial(u, v, w, p)}{\partial x} = 0 \qquad (25)$$

- Tunnel wall boundary: the normal component of the velocity is equal to zero, and the first derivatives of velocity and pressure with respect to the direction normal to the tunnel wall are taken equal to zero.

$$\frac{\partial(p, \vec{q}_t)}{\partial n} = 0 \qquad (26)$$

$$\vec{q} \cdot \vec{n} = 0 \qquad (27)$$

where $\vec{q}$ is the total velocity defined as $\vec{q} = (u, v, w)$, and $\vec{q}_t$ is the tangential component of the total velocity.

Multi-block method

Since the effect of the rudder on the propeller could be significant in the case the blockage effects due to the rudder alter the inflow to the propeller, the propeller-rudder interaction needs to be considered. In this paper, the propeller-rudder interaction is evaluated by using a multi-block approach in Euler solver. As shown in Fig. 4, the multi-block method divides the fluid domain into two blocks, i.e., one block for the flow around the propeller represented by body force and another block for the flow around the rudder represented as a solid boundary [Natarajan 2003]. The overlapping zone is introduced to improve the convergence of the iterative process between the two blocks. Two blocks communicate to each other through the exchange of velocities and pressure.
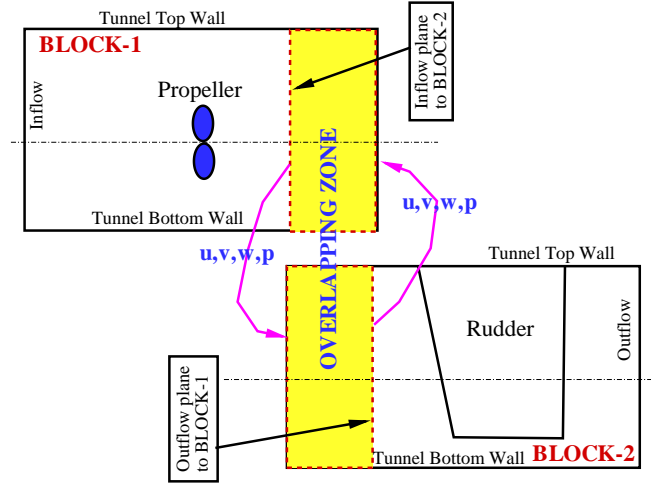
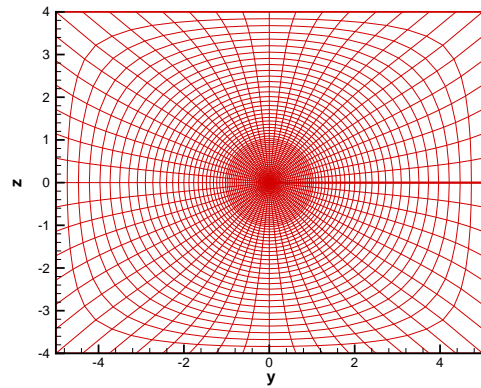

Figure 4: Two blocks used in the 3-D Euler solver

Figure 5: Cylindrical grid used in block-1 at the inflow plane for block-2 (as shown in Figure 4). Looking from downstream.

The multi-block method is composed of two iterative processes: An iteration between the propeller solver (MPUF-3A) and the 3-D Euler solver, and an iteration between block-1 and block-2. A cylindrical grid is used in block-1 (Fig. 5) to accommodate the body force cells representing the propeller, whereas an H-type adapted grid is used to model the rudder in block-2 (Fig. 6).

The iterative process between block-1 and block-2 is as follows:

- In block-1

  - Perform the propeller analysis using the measured nominal wake as the inflow, and find the loading of propeller (MPUF-3A).

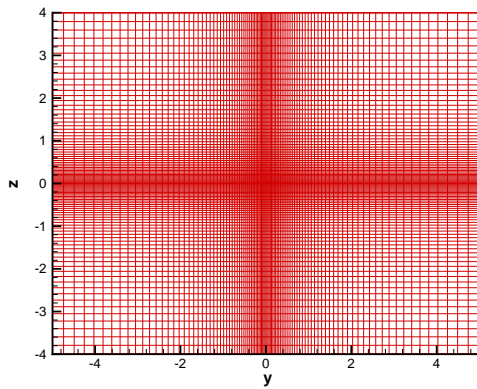 - Solve the velocity flow field by using the

Figure 6: H-type grid used in block-2 at the outflow plane for block-1 (as shown in Figure 4). Looking from downstream.
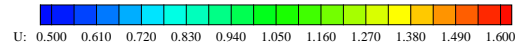

Figure 7: Axial velocity (u) contours at the center-plane of the domain as predicted by GBFLOW-3D/MPUF-3A in the absence of rudder: uniform inflow.

body forces computed from the propeller solver (MPUF-3A).

– Compute the effective wake by subtracting the induced velocity from the total velocity obtained from the Euler method.

– Interpolate velocities and pressure along the overlapping zone into the inflow boundary for block-2.

• In block-2

– Compute the velocity flow field around rudder using the interpolated inflow conditions.

– Interpolate velocities and pressure into the outflow boundary for block-1.

• Solve block-1 problem using the computed effective wake for MPUF-3A run, and update the propeller loading.

• Do iterations between block-1 and block-2 until the propeller loading converges.

VALIDATIONS AND RESULTS

Convergence studies

In order to validate the present method, the sensitivity of the solution to varying number of panels is studied for a cavitating rudder subject to the flow field shown in Figs. 7 and 8. The flow field shown in Figs. 7 and 8 is evaluated from the iterative runs between GBFLOW-3D and MPUF-3A, and tunnel walls are modeled as solid boundaries in GBFLOW-3D, and using quadrilateral panels in PROPCAV. The dimensions of the computational domain

and half of its grid are shown in Fig. 9. The tunnel top wall is located at $Y = 1.756R$ (R = propeller radius), and the tunnel bottom wall is located at $Y = -1.756R$. The mid-chord line of the rudder is located at $X = 1.4234R$ downstream of propeller, and the span of the rudder is extended from tunnel top wall to $Y = -1.06R$. The cavitation number, $\sigma_R = 2.0$, and Froude number, F_R [‡] $= 1.5$, are used for the convergence tests. The rudder turning angle, α is 2° toward the starboard side. The convergence of the circulation distribution of the cavitating rudder with varying spanwise and chordwise number of panels is shown in Figs. 10 and 11, respectively. A full-cosine spacing along the chordwise direction and the uniform spacing along the spanwise direction are used for paneling of the rudder. As shown in Figs. 10 and 11, the circulation distribution converges very quickly with number of chordwise and spanwise panels. Figure 12 depicts the convergence of cavity volume with number of panels on the rudder. As shown in the figure, the cavity volume prediction is somewhat sensitive to the number of panels. The dependence of cavity planforms on the panel discretization is shown in Fig. 13, where the cavity planforms are shown not to be much sensitive to the number of panels.

Validation with experiment

The predicted cavity patterns are compared with those observed from the experiments to validate the numerics of the present method. The experiment has been conducted for a horn-type rudder in the presence of a 6-bladed propeller inside a cavitation tunnel. Figure 14 depicts the dimension and the arrangement of propeller, rudder and cavitation tunnel.

In the experiment, the propeller operates at a de-

[‡] $F_R = V_{ship}^2/gS$. g is the gravitational force and S is the span of rudder.

TUNNEL DIMENSION
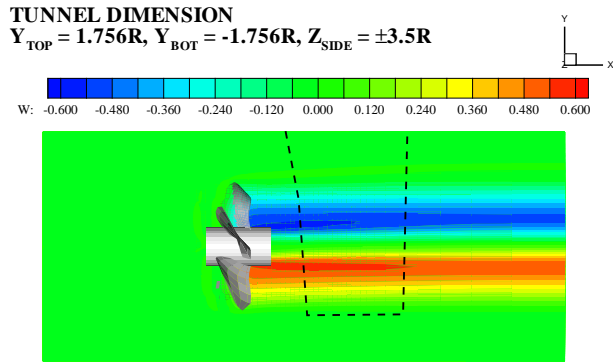**$Y_{TOP} = 1.756R$, $Y_{BOT} = -1.756R$, $Z_{SIDE} = \pm3.5R$**

Figure 8: Circumferential velocity (w) contours at the center-plane of the domain as predicted by GBFLOW-3D/MPUF-3A in the absence of rudder: uniform inflow.
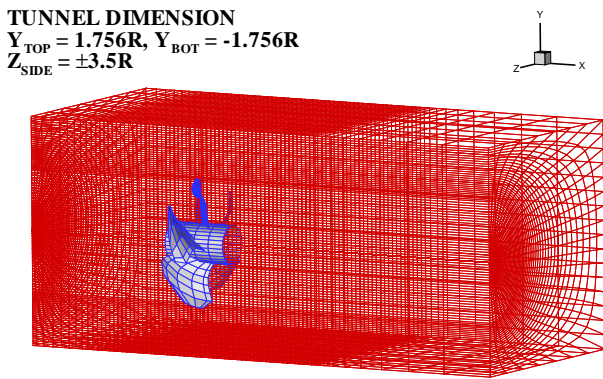
TUNNEL DIMENSION
$Y_{TOP} = 1.756R$, $Y_{BOT} = -1.756R$
$Z_{SIDE} = \pm3.5R$

Figure 9: Computational domain used in GBFLOW-3D/MPUF-3A with the tunnel walls and the propeller.
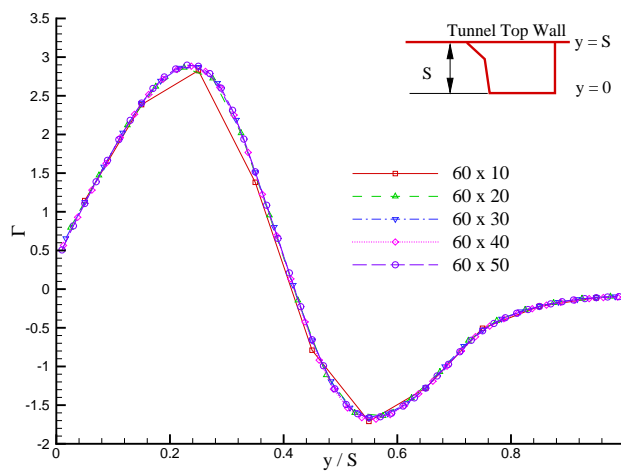
Figure 10: Convergence of circulation distribution on cavitating rudder with spanwise number of panels: $\sigma_R = 2.0$, $F_R = 1.5$, and $\alpha = 2^o$.
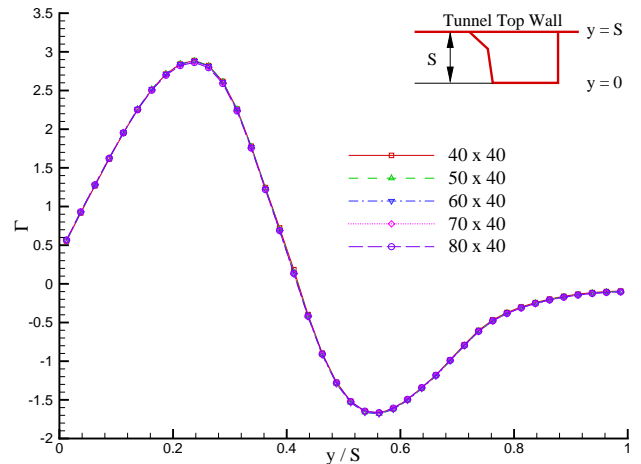
Figure 11: Convergence of circulation distribution on cavitating rudder with chordwise number of panels: $\sigma_R = 2.0$, $F_R = 1.5$, and $\alpha = 2^o$.
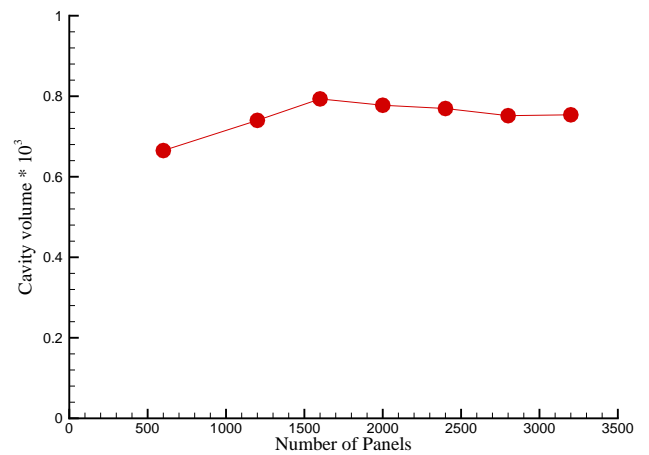
Figure 12: Convergence of cavity volume on the rudder with number of panels: $\sigma_R = 2.0$, $F_R = 1.5$, and $\alpha = 2^o$.
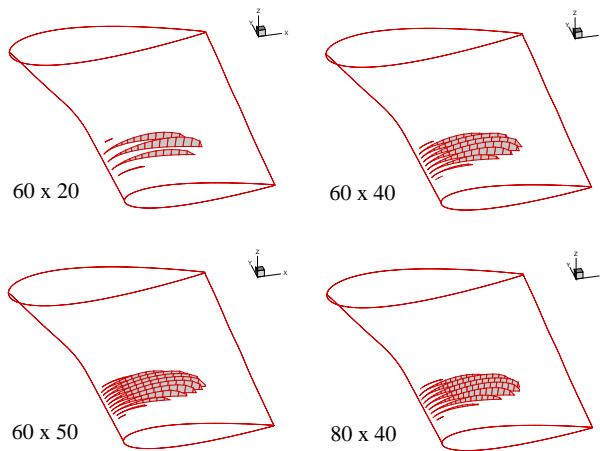
Figure 13: Convergence of cavity planform on the rudder with number of panels: $\sigma_R = 2.0$, $F_R = 1.5$, and $\alpha = 2^o$.

Figure 14: Configuration of propeller and horn type rudder inside of a tunnel.

sign advance ratio of $J_s = 0.96$ with thrust coefficient, $K_T = 0.2012$. In this computation, the propeller advance ratio is adjusted so that the resulting thrust coefficient matches the value of the design thrust coefficient measured from experiment. The advance ratio corresponding to the design $K_T = 0.2012$ is determined through trial and error, and $J_s = 1.07$ is used for the computation. The measured nominal axial velocity at the propeller plane is shown in Fig. 15. The effective wake predicted by GBFLOW-3D and MPUF-3A is shown in Fig. 16, where the interaction between the propeller and the tunnel is included in an iterative manner. The axial and circumferential velocity contours at the center plane of the domain are shown in Figs. 17 and 18, respectively. As shown in Fig. 18, the circumferential velocity varies from positive below the propeller shaft to negative above the propeller shaft axis over the rudder in the propeller slipstream. The predicted pressure contours are shown in Fig. 19, where the expected pressure jump across the propeller plane is clearly shown in the figure.

Figures 20 and 21 show the observed and the predicted cavity patterns at the cavitation numbers, $\sigma_R = 1.24$ and 1.65, and the rudder turning angle, $\alpha = 5^o$. The rudder turning angle toward the starboard side is considered to be positive in the experiment. As shown in the figures, the predicted cavity patterns are well compared with those observed.

The effect of propeller and tunnel walls on rudder cavitation

The effect of propeller and tunnel walls on rudder cavitation is shown in Fig. 22. The inflow to the rudder in the case of with tunnel and propeller effect is shown in
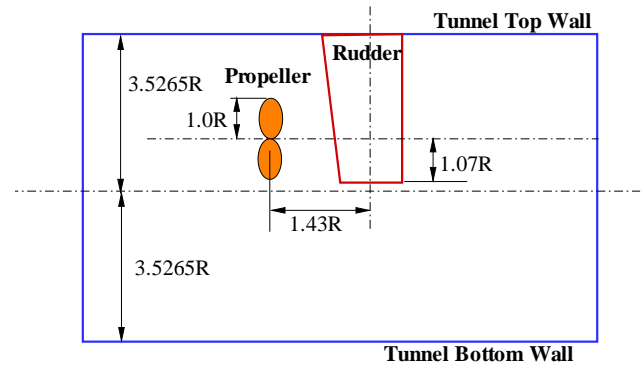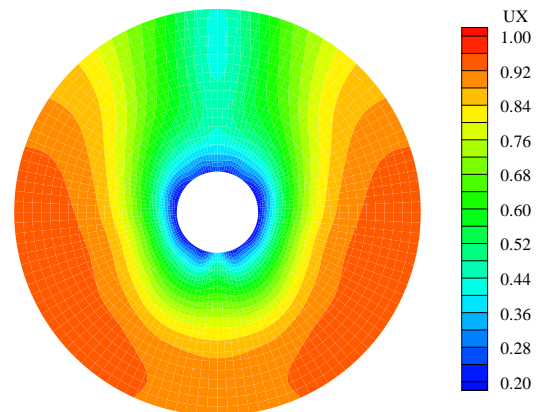

Figure 15: Axial velocity contours of nominal wake measured from experiment.
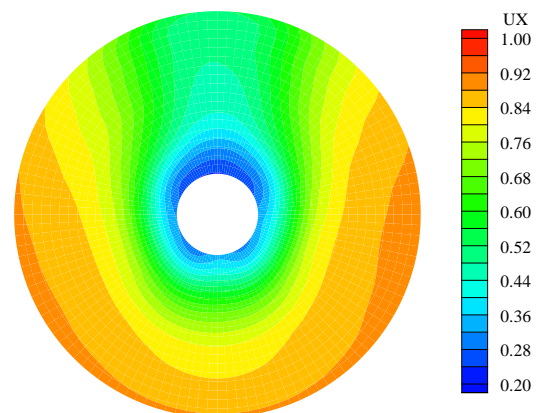

Figure 16: Axial velocity contours of effective wake predicted from GBFLOW-3D/MPUF-3A run: the effective wake is computed at $x = -0.3$ location.
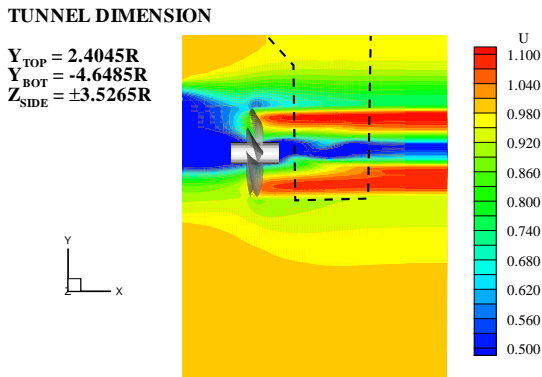
Figure 17: Axial velocity (u) contours at the center-plane of the domain as predicted by GBFLOW-3D/MPUF-3A in the absence of rudder.
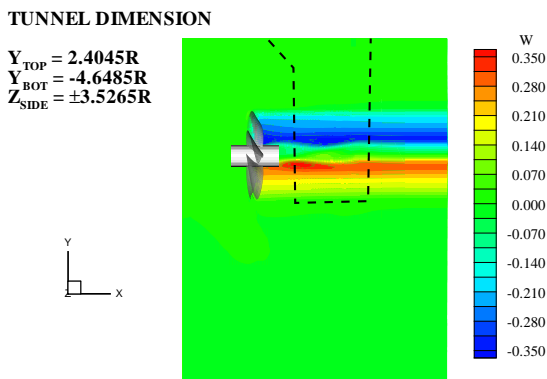

Figure 18: Circumferential velocity (w) contours at the center-plane of the domain as predicted by GBFLOW-3D/MPUF-3A in the absence of rudder.
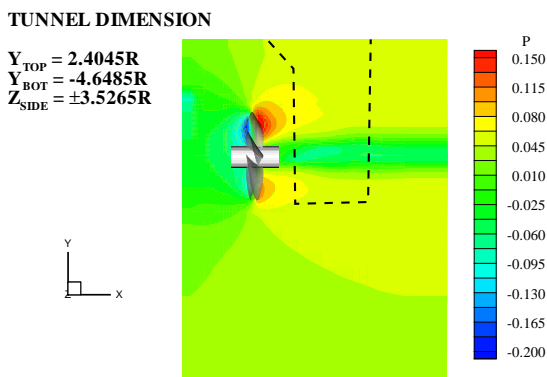

Figure 19: Pressure contours at the center-plane of the domain as predicted by GBFLOW-3D/MPUF-3A in the absence of rudder. The shown pressure does not include the hydrostatic terms.
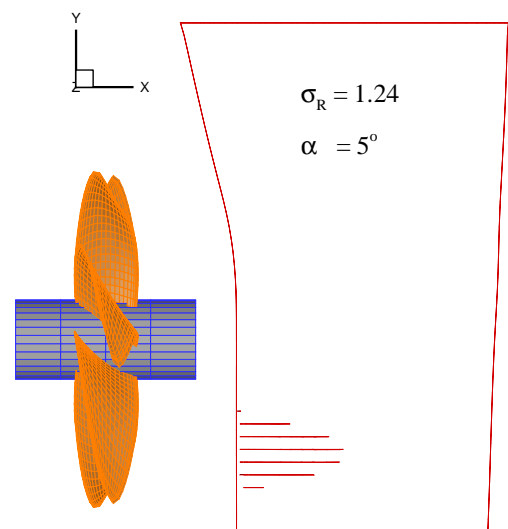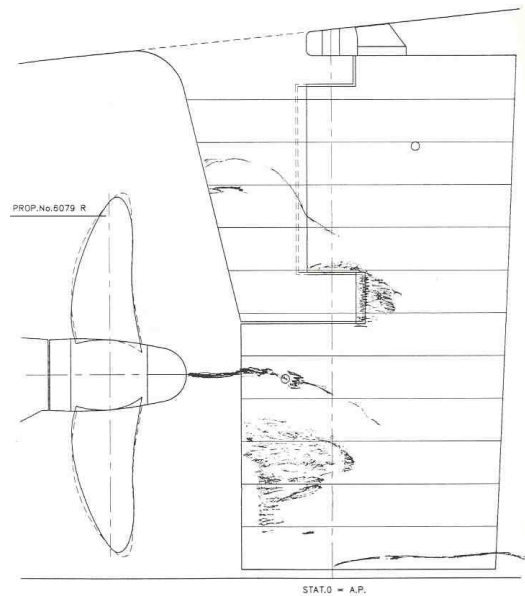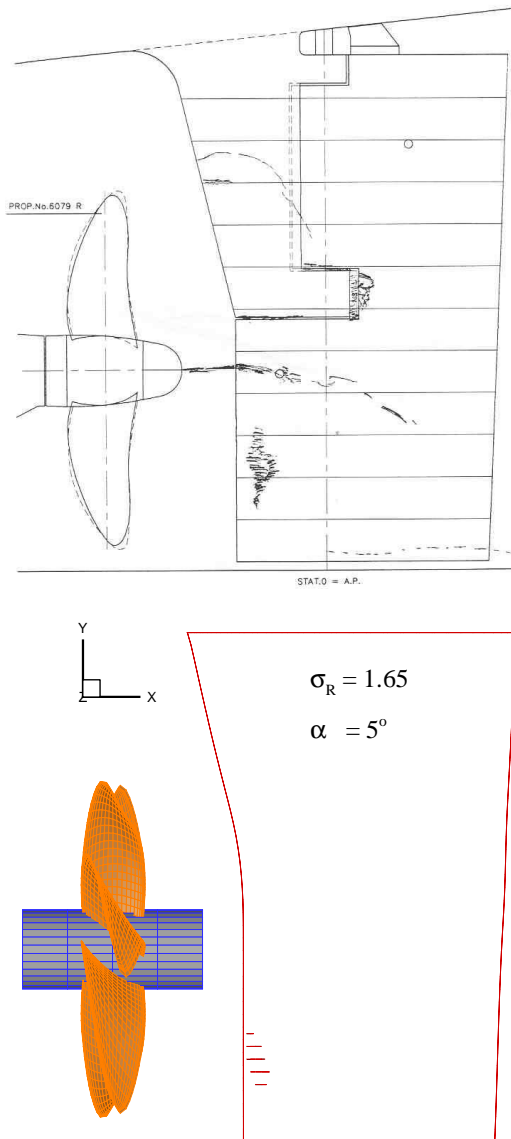

Figure 20: Comparison of cavity patterns observed from experiment (top) and predicted by PROPCAV (bottom) with tunnel effect: $\sigma_R = 1.24$, $F_R = 1.5$, and $\alpha = 5^o$.

(a) Without propeller and without tunnel Effect

(b) with propeller and without tunnel effect

(c) with propeller and with tunnel effect

(d) with propeller and with tunnel effect
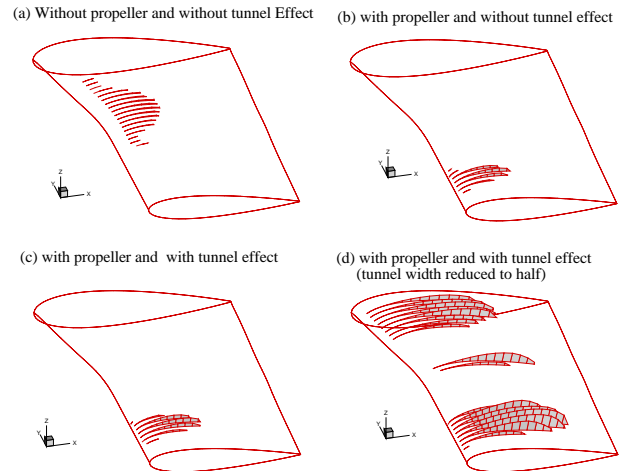(tunnel width reduced to half)

Figure 22: Comparison of the cavity patterns predicted by PROPCAV with/without propeller and/or tunnel effect: (a) without propeller and without tunnel effect, (b) with propeller and without tunnel effect, (c) with propeller and with tunnel effect, and (d) with propeller and with tunnel effect with reduced tunnel width by half; $\sigma_R = 1.24$, $F_R = 1.5$, and $\alpha = 5^o$

Figs. 17 and 18. The variation of circumferential velocity induces varying angle of attack to the rudder section, and that changes the loading on the rudder, as shown in Fig. 23. The rudder loading below the propeller shaft increases due to the positive circumferential velocity, and as a result of that, the cavity extent increases. On the other hand, the cavity disappears above the propeller shaft axis (Fig. 22-(b) and (c)). As the tunnel side wall distance decreases, the sheet cavity grows over the rudder (Fig. 22-(d)) due to the increased loading of the flow.

Validation of Multi-block scheme

The propeller-rudder interaction is performed for a horn-type rudder with NACA00 thickness form and 20% thickness to chord ratio. The computational domain used is shown in Fig. 24. In Fig. 25 the axial velocity distribution is shown along the center plane, where the effect of the rudder is clearly shown. Figure 26 shows the circumferential velocity contours along the center plane for both blocks. From this figure it can be seen clearly that the vortical flow induced by the propeller is canceled downstream of the rudder trailing edge. The presence of the rudder causes a decrease in the axial velocity at an axial location upstream of the rudder. The convergence of the propeller thrust and the torque coefficients with number of iterations is shown in Fig. 27.
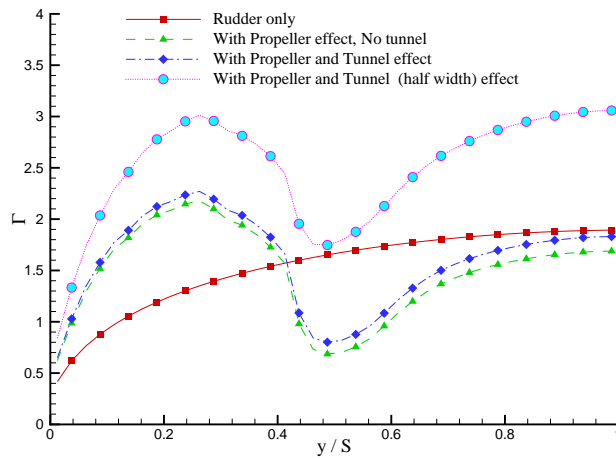

$\sigma_R = 1.65$

$\alpha = 5^o$

Figure 21: Comparison of cavity patterns observed from experiment (top) and predicted by PROPCAV (bottom) with tunnel effect: $\sigma_R = 1.65$, $F_R = 1.5$, and $\alpha = 5^o$.

Figure 23: Comparison of the circulation distribution predicted by PROPCAV with/without propeller and/or tunnel effect: (a) without propeller and without tunnel effect, (b) with propeller and without tunnel effect, (c) with propeller and with tunnel effect, and (d) with propeller and with tunnel effect with reduced tunnel width by half; $\sigma_R = 1.24$, $F_R = 1.5$, and $\alpha = 5^o$
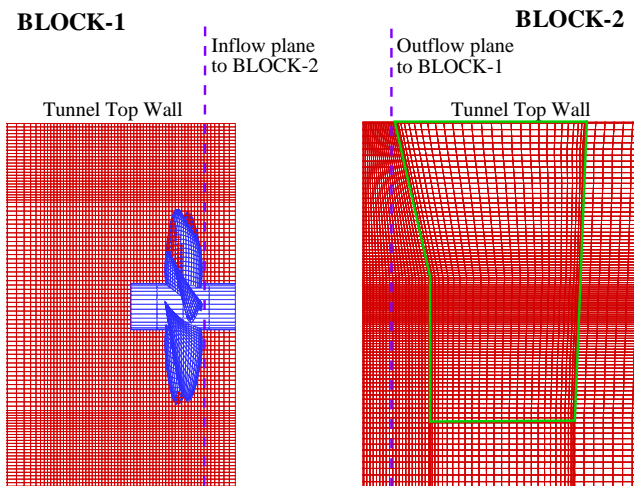

Figure 25: Axial velocity (u) contours on the center plane of block-1 and 2 for a horn-type rudder.

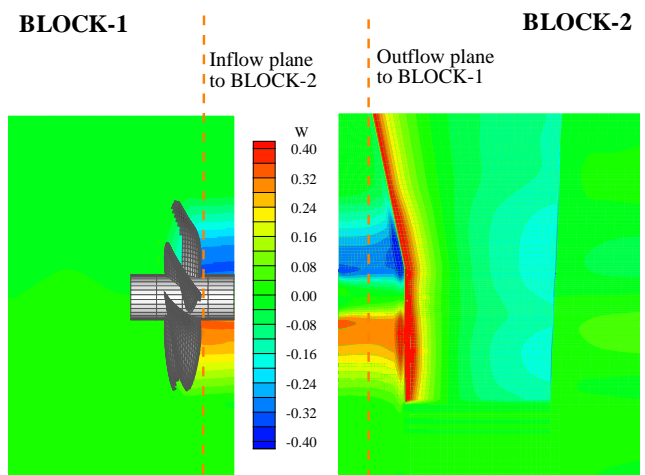Figure 24: 3-D Euler solver grid showing horn-type rudder with NACA0020 section.

Figure 26: Circumferential velocity (w) contours on the center plane of block-1 and 2 for a horn-type rudder.
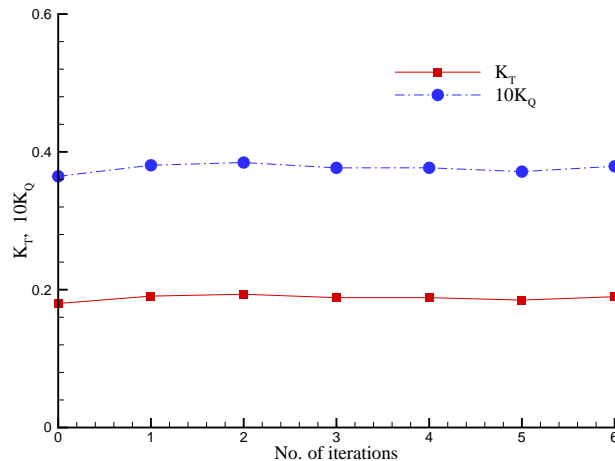
Figure 27: Convergence of propeller forces with the number of iterations.

CONCLUSIONS

A low-order boundary element method (PROPCAV), a vortex-lattice method (MPUF-3A) and a steady three-dimensional Euler solver (GBFLOW-3D) have been coupled to predict the sheet cavitation over the rudder subject to an inflow induced by propeller inside a tunnel. Iterations between GBFLOW-3D and MPUF-3A were performed to predict the effective wake to the propeller and the new loading on the propeller. The tunnel walls were treated as solid boundaries, and the rudder was not modeled in GBFLOW-3D. The propeller total flow field was computed by GBFLOW-3D at the rudder control points. The rudder sheet cavitation was predicted by PROPCAV using the inflow induced by propeller, and the effect of the tunnel walls were considered in an iterative manner.

The present method was validated by performing the several convergence studies with varying number of panels, and by comparing the predicted cavity patterns with those observed in an experiment at a cavitation tunnel. The predicted cavity patterns by the present method compared well with those observed in the experiment. The multiblock scheme which accounts for the two-way interaction between the rudder and the propeller was also developed and preliminary results were presented.

ACKNOWLEDGMENT

References

Achkinadze, A. S., Berg, A., Krasilnikov, V. I., and Stepanov, I. E. (2003). Numerical analysis of podded and steering system using a velocity based source boundary element method with modified trailing edge. In *Propellers/Shafting 2003 Symposium*, pages 1–22 (paper No. 12), Virginia Beach, VA. Soc. Naval Arch. & Marine Engnrs.

Breslin, J. P., Van Houten, R. J., Kerwin, J. E., and Johnsson, C.-A. (1982). Theoretical and experimental propeller-induced hull pressures arising from intermittent blade cavitation, loading, and thickness. *Trans. of Society of Naval Architects & Marine Engineers*, 90:111–151.

Choi, J.-K. (2000). *Vortical Inflow – Propeller Interaction Using Unsteady Three-Dimensional Euler Solver*. PhD thesis, Department of Civil Engineering, The University of Texas at Austin.

Choi, J.-K. and Kinnas, S. A. (1998). A 3-D Euler Solver and Its Application on the Analysis of Cavitating Propellers. In *25th American Towing Tank Conference*, Iowa City, IA.

Choi, J.-K. and Kinnas, S. A. (2000a). Non-axisymmetric effective wake prediction by using an unsteady three-dimensional Euler solver. In *Propellers/Shafting '00 Symposium*, Virginia Beach, VA. Soc. Naval Arch. & Marine Engnrs.

Choi, J.-K. and Kinnas, S. A. (2000b). An unsteady three-dimensional euler solver coupled with a cavitating propeller analysis method. In *The 23rd Symposium on Naval Hydrodynamics*, Val de Reuil, France.

Choi, J.-K. and Kinnas, S. A. (2001). Prediction of non-axisymmetric effective wake by a 3-D Euler solver. *Journal of Ship Research*, 45(1):13–33.

Choi, J.-K. and Kinnas, S. A. (2003). Prediction of unsteady effective wake by a euler solver/vortex-lattice coupled method. *Journal of Ship Research*, 47(2):131–144.

Chorin, A. J. (1967). A numerical method for solving incompressible viscous flow problems. *Journal of Computational Physics*, 2:pp.12–26.

Fine, N. E. (October, 1992). *Nonlinear Analysis of Cavitating Propellers in Nonuniform Flow*. PhD thesis, Department of Ocean Engineering, MIT.

Fine, N. E. and Kinnas, S. A. (1993a). A boundary element method for the analysis of the flow around 3-d cavitating hydrofoils. *Journal of Ship Research*, 37:213–224.

Fine, N. E. and Kinnas, S. A. (1993b). The nonlinear numerical prediction of unsteady sheet cavitation for propellers. In *Sixth International Conference On Numerical Ship Hydrodynamics*, pages 531–544, University of Iowa, Iowa.

Han, J., Kong, D., Kim, Y., and Lew, J. (1999). Analysis of propeller-rudder interaction with rudder angle. *Annual Autumn Meeting of SNAK, Taejon, Korea*, pages pp. 206–209.

Han, J., Kong, D., Song, I.-H., and Lee, C.-S. (2001). Analysis of cavitating flow around the horn-type rudder in the race of a propeller. *Fourth International Symposium on Cavitation, California Institute of Technology, Pasadena, CA USA, CAV2001:sessionB9.005*.

Kerwin, J. E., Kinnas, S. A., Wilson, M. B., and J., M. (1986). Experimental and analytical techniques for the study of unsteady propeller sheet cavitation. In *Sixteenth Symposium on Naval Hydrodynamics*, Berkeley, California.

Kerwin, J. E. and Lee, C.-S. (1978). Prediction of Steady and Unsteady Marine Propeller Performance by Numerical Lifting-Surface Theory. *Trans. of Society of Naval Architects & Marine Engineers*, 86:218–253.

Kinnas, S. A. (1985). Non-linear corrections to the linear theory for the prediction of the cavitating flow around hydrofoils. Technical Report 85-10, MIT, Department of Ocean Engineering.

Kinnas, S. A. (1991). Leading-edge corrections to the linear theory of partially cavitating hydrofoils. *Journal of Ship Research*, 35(1):pp. 15–27.

Kinnas, S. A., Choi, J.-K., Kosal, E. M., Young, Y. L., and Lee, H. S. (1999). An integrated computational technique for the design of propellers with specified constraints on cavitation extent and hull pressure fluctuations. In *CFD99 - The International CFD Conference*, Ulsteinvik, Norway.

Kinnas, S. A., Choi, J.-K., Lee, H. S., and Young, Y. L. (2000). Numerical cavitation tunnel. In *NCT50, International Conference on Propeller Cavitation*, pages 137–157, Newcastle upon Tyne, England.

Kinnas, S. A. and Fine, N. E. (1989). Theoretical prediction of the midchord and face unsteady propeller sheet cavitation. In *Fifth International Conference on Numerical Ship Hydrodynamics*, pages 685–700, Hiroshima, Japan.

Kinnas, S. A. and Fine, N. E. (1992). A nonlinear boundary element method for the analysis of unsteady propeller sheet cavitation. In *Nineteenth Symposium on Naval Hydrodynamics*, pages 717–737, Seoul, Korea.

Kinnas, S. A. and Fine, N. E. (1993). A numerical nonlinear analysis of the flow around 2-d and 3-d partially cavitating hydrofoils. *Journal of Fluid Mechanics*, 254:151–181.

Kinnas, S. A., Griffin, P. E., Choi, J.-K., and Kosal, E. M. (1998a). Automated design of propulsor blades for high-speed ocean vehicle applications. *Trans. of Society of Naval Architects & Marine Engineers*, 106:213–240.

Kinnas, S. A., Griffin, P. E., and Mueller, A. C. (1997). Computational tools for the analysis and design of high speed propulsors. In *The International CFD Conference*, Ulsteinvik, Norway.

Kinnas, S. A., Lee, H. S., and Mueller, A. C. (1998b). Prediction of propeller blade sheet and developed tip vortex cavitation. In *22nd Symposium on Naval Hydrodynamics*, pages 182–198, Washington, D.C.

Kinnas, S. A., Natarajan, S., Lee, H. S., Kakar, K., and Gupta, A. (2003). Numerical modeling of podded propulsors and rudder cavitation. In *Propellers/Shafting 2003 Symposium*, pages 1–20 (paper No. 5), Virginia Beach, VA. Soc. Naval Arch. & Marine Engnrs.

Kudo, T. and Kinnas, S. A. (1995). Application of unsteady vortex/source lattice method on supercavitating propellers. In *24th American Towing Tank Conference*, pages 33–40, Texas A&M University.

Lee, C. (1979). *Prediction of Steady and Unsteady Performance of Marine Propellers with or without Cavitation by Numerical Lifting Surface Theory*. PhD thesis, M.I.T., Department of Ocean Engineering.

Lee, C.-S. (1981). Prediction of the transient cavitation on marine propellers. In *Thirteenth Symposium on Naval Hydrodynamics*, pages 41–64, Tokyo, Japan.

Lee, H. S. (2002). *Modeling of Unsteady Wake Alignment and Developed Tip Vortex Cavitation*. PhD thesis, Department of Civil Engineering, The University of Texas at Austin.

Lee, H. S., Gu, H., Natarajan, S., and Kinnas, S. A. (2003). MPUF-3A (version 2.1) user's manual. Ocean Engineering Report 03-2, Ocean Engineering Group, UT Austin, Austin, TX.

Lee, H. S. and Kinnas, S. A. (2001). Modeling of unsteady blade sheet and developed tip vortex cavitation. In *CAV 2001: Fourth International Symposium on Cavitation*, Pasadena, CA. California Institute of Technology.

Lee, H. S. and Kinnas, S. A. (2003). Application of bem in the prediction of unsteady blade sheet and developed tip vortex cavitation on marine propellers. *Journal of Ship Research*, Accepted for publication.

Mueller, A. C. (1998). Development of face and mid-chord cavitation models for the prediction of unsteady cavitation on a propeller. Master's thesis, UT Austin, Dept. of Civil Engineering.

Mueller, A. C. and Kinnas, S. A. (1997). Cavitation predictions using a panel method. In *ASME Symposium on Marine Hydrodynamics and Ocean Engineering*, volume 14, pages 127–137, Dallas, TX.

Mueller, A. C. and Kinnas, S. A. (1999). Propeller sheet cavitation predictions using a panel method. *Journal of Fluids Engineering*, 121:282–288.

Natarajan, S. (2003). Computational modeling of rudder cavitation and propeller/rudder interaction. Master's thesis, The University of Texas at Austin.

Ni, R.-H. (1982). A multiple-grid scheme for solving the Euler equations. *AIAA Journal*, 20(11):pp.1565–1571.

Shen, Y., Remmers, K., and Jiang, C. W. (1997). Effects of ship hull and propeller on rudder cavitation. *Journal of Ship Research, Vol. 41, No. 3, pp.172 180*.

Tamashima, M., Matsui, S., Yang, J., Mori, K., and Yamazaki, R. (1993). The method for predicting the performance of propeller-rudder system with rudder angles and its application to the rudder design. *Transaction of the West-Japan Society of Naval Architects*, 86:pp. 53–76 (in Japanese).

Tulin, M. P. and Hsu, C. C. (1980). New applications of cavity flow theory. In *13th Symposium on Naval Hydrodynamics*, Tokyo, Japan.

Uhlman, J. S. (1987). The surface singularity method applied to partially cavitating hydrofoils. *Journal of Ship Research*, 31(No. 2):107–124.

Young, Y. L. (2002). *Numerical Modeling of Supercavitating and Surface-Piercing Propellers*. PhD thesis, Department of Civil Engineering, The University of Texas at Austin.

Young, Y. L. and Kinnas, S. A. (1999). Numerical and experimental validation of a cavitating propeller bem code. In *Cavitation and Multiphase Flow Forum*, San Fransisco, CA. 3rd ASME/JSME Joint Fluids Engineering Conference.

Young, Y. L. and Kinnas, S. A. (2001). A bem for the prediction of unsteady midchord face and/or back propeller cavitation. *Journal of Fluids Engineering*, 123(2):311–319.

Young, Y. L. and Kinnas, S. A. (2002). A bem technique for the modeling of supercavitating and surface-piercing propeller flows. In *The 24rd Symposium on Naval Hydrodynamics*, Fukuoka, Japan.

Young, Y. L. and Kinnas, S. A. (2003). Numerical modeling of supercavitating propeller flows. *Journal of Ship Research*, 47(1):48–62.